Physicochemical Insights into Microscopic Events Driven by GTP Hydrolysis Reaction in Ras-GAP system

Ikuo Kurisaki[*1], Shigenori Tanaka[*1]

[1]Department of Computational Science, Graduate School of System Informatics, Kobe University, 1-1 Rokkodai-cho, Nada-ku, Kobe 657-8501, Japan

[*]Ikuo Kurisaki

E-mail: kurisaki@bear.kobe-u.ac.jp, Tel: +81-78-803-6472

[*]Shigenori Tanaka

E-mail: tanaka2@kobe-u.ac.jp, Tel: +81-78-803-6620

Abstract

Hydrolysis reaction of nucleotide triphosphate, ATP and GTP in particular, has been widely found as regulatory machinery for protein functional expression in the cell. Nonetheless, the microscopic mechanisms for functional regulations via the chemical reactions are mostly elusive so far, due to technical difficulty of both experimental observations and conventional theoretical simulations. We addressed the problem by examining the conjecture that Coulomb repulsion interaction between products, ADP/GDP and inorganic phosphate (P_i), execute the mechanical works upon the system. GTP hydrolysis reaction for Ras-GTP-GAP system was effectively simulated in the framework of classical atomistic molecular dynamic simulations by switching force field parameters between the reactant and product systems. We observed transient increase of kinetic energy of GDP and P_i, and the neighboring functional domains of Ras. One of such functional regions, P-loop, shows increase of nonbonded potential energy, which is retained even after gained kinetic energy is dissipated. This change is explained from rearrangement of hydrogen bonding between P-loop and GDP. Interestingly, even if increase of kinetic energy is suppressed, the above change is reproduced through GTP-GDP conversion. This observation suggests that conversion of chemical species itself plays essential roles in regulation rather than transient heat generation via the hydrolysis

reactions.

Introduction

Various ATPase and GTPase function to regulate cellular processes such as cell mobility[1,2], molecular channeling and transporting[3], protein synthesis[4], signal transduction[5,6] and so on. It has been widely known that the hydrolysis reactions of nucleotide triphosphate are essential steps for their functional expression, while it is not understood satisfactorily from the microscopic viewpoint how such chemical reactions generate mechanical works available for their functional expression.

Knowledge for heat generation of several kcal/mol associated with the hydrolysis has been often remarked as the basis for physicochemical investigation for the molecular mechanism. Nonetheless, it should be noted that this macroscopic, thermodynamic quantity denotes total free energy balance of the reaction, which is obtained from accumulation of any energetic processes (microscopic heat generation, rearrangements of solvation shell and configurational change of biomacromolecules and so on), thus not necessarily explaining how generated work drives molecular dynamics of proteins. Thus microscopic mechanisms for work generation via these hydrolysis reactions are in general elusive. This is due to experimental difficulty to observe substantially fast, sub-picosecond dynamics with sufficient spatial and temporal resolution.[7,8]

Molecular simulations are expected as a technical counterpart because of the finer

temporal resolution combined with atomic resolution, while it should be noted that chemical reactions are still 'rare events' for conventional atomistic simulations. Actually, the reaction times of ATPase and GTPase are usually 1000-fold longer or more than the simulation time length accessible with available computational resources of today[9]. It is thus challenging to extend the dynamics of molecular systems to the time domain where such a fairly fast event occurs, by using brute-force MD simulation approaches.

One example of GTPase proteins is rat sarcoma (Ras). This protein is a monomeric GTPase involved in regulation of cellular signal transduction and the reaction time of GTP hydrolysis by Ras is found around several seconds even under interaction with its own GTPase activation protein (GAP).[10]

Considering the above circumstances, a feasible approach is to examine a specific physicochemical process, which is accessible by conventional molecular dynamic simulations and important to understand microscopic roles of the reaction process for mechanical work generation.

The above observation reminds us of the conjecture that ADP and inorganic phosphate (P_i) (or GDP and P_i) obtain kinetic energy via Coulomb repulsion interaction between them, collide with neighboring chemical groups in proteins, and execute mechanical works upon the system.[11] Since the estimated value of the work in this conjecture is as

much as a half of the heat generation via the hydrolysis reaction at maximum, examining this conjecture appears to give a clue to microscopically understand how the hydrolysis reaction generates mechanical work to drive functional expression of biomacromolecules. Meanwhile, to our best knowledge, there are no earlier studies to directly examine this conjecture.

In the present study, we examine the above conjecture to give deeper physicochemical insights into microscopic events driven by hydrolysis of nucleotide triphosphate in protein systems. To verify the above conjecture, we focus on 'switching force fields in molecular dynamics simulation' method, referred to as SF2MD hereafter. This kind of methods was already applied to the myoglobin heme-CO dissociation reaction due to technical advantage of SF2MD in simple implementation to existing MD simulation packages and reasonable computational costs equal to classical MD simulations.[12, 13] The earlier study considered break of single chemical bond between heme and CO and succeeded in revealing the microscopic heat transduction pathways.[12]

We apply atomistic molecular dynamics simulations with SF2MD to GTP hydrolysis reaction of Ras-GTP-GAP system (**Figure 1A**). Upon considering hydrolysis of triphosphate nucleotide, firstly we extend the earlier SF2MD scheme to be applicable for complicated reaction process. Then we analyze the physicochemical processes via

relaxation of Coulomb repulsive interaction acting between GDP and P_i and investigate the effects on functional regions of Ras protein (**Figure 1B**). Finally, we discuss the essential roles of the hydrolysis reaction for the observed changes of this protein.

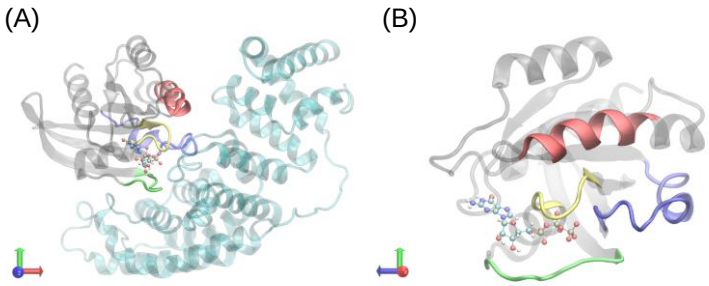

Figure 1. (A) Illustration of Ras-GTP-GAP complex and (B) magnified view of Ras and GTP. Ras and GAP proteins are represented with ribbon, while GTP is drawn by ball and stick. Functional region of Ras is highlighted with different colors as follows, yellow: P-loop; green: Switch-I; blue: Switch-II; red: α-helix 3.

Materials and Methods

Simulation setup

To calculate the forces acting among atoms, AMBER force field 14SB[14], TIP3P water model[15,16], and JC ion parameters adjusted for the TIP3P water model[17,18] were applied for amino acid residues, water molecules, and ions, respectively. Nucleotide triphosphate/diphosphates (GDP/GTP) and Mg^{2+} were described by employing the force

field parameters developed by Meagher[19] and Allnér[20], respectively.

We here considered doubly protonated inorganic phosphate (referred to as $H_2PO_4^-$ or P_i, hereafter) as the product of GTP hydrolysis reaction, according to the earlier QM/MM studies[21]. Atomic charges of P_i were derived by employing RESP charge calculation with Hartree-Fock/6-31G* level of theory using Gaussian09[22] (see **Table S1** and **Figure S1** for details). Other force field parameters of P_i were derived from general amber force field 2.[23]

All simulations were performed under the periodic boundary condition. Electrostatic interaction was treated by the Particle Mesh Ewald method, where the real space cutoff was set to 9 Å. The vibrational motions associated with hydrogen atoms were frozen by the SHAKE algorithm. The translational center-of-mass motion of the whole system was removed by every 500 steps to keep the whole system around the origin, avoiding the overflow of coordinate information from the MD trajectory format.

Construction of Ras-GTP-GAP system

We used the X-ray crystallographic structure of Ras-GDP-GAP complex (PDB entry: 1WQ1[24]) to construct a set of atomic coordinates for Ras-GTP-GAP system. Water molecules in the crystal and the bound Mg^{2+} were retained. The atomic coordinates of the

aluminum fluoride bound to Ras protein is employed to give those of γ-phosphate for the GTP system. Nε protonation state was employed for each of histidine residues, and all carboxyl groups in aspartate and glutamate residues were set to the deprotonated state. The one disulfide bond in GAP was formed according to the X-ray crystallography study[24]. The additional details for system construction are described in Supporting Information (*see* **SI 1**).

MD simulations for structure relaxation

Following temperature relaxation with NVT simulations, 20-ns NPT MD simulations (300 K, 1 bar) were performed and used for structural relaxation. The system temperature and pressure were regulated with Berendsen thermostat[25] with a 5-ps of coupling constant and Berendsen barostat[25] with a 0.1-ps coupling constant, respectively. A set of initial atomic velocities were randomly assigned from the Maxwellian distribution at 0.001 K at the beginning of the NVT simulations. The time step of integration was set to 2 fs. This simulation procedure was repeated fifty times by assigning different initial atomic velocities. Each of MD simulations was performed using the Amber 17[26] GPU-version PMEMD module based on SPFP algorism[27] with NVIDIA GeForce GTX1080Ti. The further technical details are given in Supporting Information (*see* **SI 2**).

MD simulation with switching force fields

Each of 20-ns NPT simulation for structural relaxation is further extended for 106 ps under NVE condition, referred to as forward NVE simulation (f-NVE) hereafter. The snapshot structure obtained from the f-NVE is employed to construct Ras-GDP-GAP system by converting GTP and reactant water (W_R) into GDP and P_i (The detailed procedure will be given in the following subsection).

The generated Ras-GDP-GAP system is simulated for 106 ps under NVE condition, referred to as backward NVE simulation (b-NVE) hereafter. Except for P_i molecule, atomic velocities are taken over from the f-NVE, while velocity vector for each of atoms in P_i are set to zero vector. This treatment is due to rearrangement of chemical bonding for P_i and technical concern about anomalous increase of the kinetic energy via relaxation of P_i structure. A b-NVE is further extended for 20 ns under NVE condition.

In f-NVE, atomic coordinates and velocities are recorded by 1 ps, 0.05 ps and 0.002 ps in the first 100 ps, next 5 ps and the last 1 ps, respectively. In b-NVE, atomic coordinates and velocities are recorded by 0.002 ps, 0.05 ps and 1 ps in the first 1 ps, next 5 ps and the last 100 ps, respectively. Finer output of trajectory information for 1-ps NVE simulations is aimed to analyze faster dynamics such as heat generation found in b-NVE.

We also performed similar NVE MD simulations for Ras-GTP-GAP system. The f-NVE is simply extended by 106-ps plus 20-ns under NVE condition without GTP-GDP conversion. The atomic velocities for P_γ in GTP and W_R were set to zero at the timing of force field switchover. This velocity modification procedure is performed for consistency with simulations for Ras-GDP-GAP system. The 106-ps NVE MD simulation, which is then extended by 20 ns under NVE condition, is referred to as reference NVE simulation (r-NVE), hereafter.

Each 106-ps NVE and the following 20-ns NVE simulations were performed by using the Amber 20[28] CPU-version PMEMD module and GPU-version PMEMD module based on SPFP algorism[27] with Tesla V100-PCIE, respectively.

Rearrangement of atomic coordinates to construct reactant system

The hydrolysis reaction accompanies both formation and breakage of chemical bonds between reactant molecules. We thus carefully treated such a complicated rearrangement of chemical bonds in contrast to the simple bond breakage discussed in the earlier studies [12,13], where we employed QM/MM method to simulate chemical conversion from reactant(GTP + reactant water (W_R)) to product (GDP + inorganic phosphate (P_i)). This technical modification should be useful to avoid anomalous steric crashes among atoms

in the product state and following unnatural heat generation unfavorably caused by relaxation of such steric crashes. Actually, we found that conventional MM methods did not work to generate P_i configuration due to fixed representation of chemical bonds (see **Figure S2** for representative structure illustration in Supporting Information).

We constructed a Ras-GDP-GAP system by using the snapshot structure obtained from each f-NVE. Positional rearrangement of atoms involved in the GTP hydrolysis reaction ($P\gamma O_3^-$ in GTP and W_R) was performed by using QM/MM methods with Amber force field 14[14] and PM3 level of theory[29]. QM/MM simulations were performed by using Amber20 built-in QM/MM interface.

The QM region consists of W_R and $P\gamma O_3^-$ in GTP, having 47 atoms in total. In this QM/MM procedure, we deleted the harmonic potential function for the interatomic bond between P_γ and $O2_\beta$ in GTP by using ParmEd in Amber20[28]. This treatment is technically necessary to define the QM region as closed-shell electronic structure in our simulation environment.

By referring to the earlier QM/MM study on GTP hydrolysis in Ras-GAP system[21], we selected a water molecule as W_R, which is found in the vicinity of P_γ in GTP (a representative configuration will appear later). To obtain atomic coordinates of product state, interatomic distances discussed in the earlier QM/MM study were constrained by

employing harmonic potential with force constant of 500000 kcal/mol/Å^2 (**Table 1**). The atom pairs were selected by recalling the earlier QM/MM study[21].

Table 1. Pairs of atoms for harmonic potentials in QM/MM simulations and the corresponding equilibrium distances.

atom 1	atom 2	equilibrium distance [Å]
Pγ in GTP	O3β in GTP	3.05
Pγ in GTP	O in W_R[†]	1.54
O1γ in GTP	H in W_R	0.96
O1β in GTP	H in W_R	1.92

[†]W_R denotes reactant water molecule.

The atomic coordinates except for those consisting of GTP and W_R are frozen with ibelly algorithms. Electrostatic interaction was treated by the Particle Mesh Ewald method, where the real space cutoff was set to 9 Å. Interactions between QM and MM regions were considered by electrostatic embedding scheme. The atomic charge in the QM region was set to −1.

Heat quenching simulations

The setup for heat quenching simulations is basically the same as that for the b-NVE.

In the heat absorption scheme, the Ras-GDP-GAP system is combined with the Langevin thermostat with 100-ps^{-1} collision coefficient during the first 1-ps of b-NVE.

Meanwhile, the energy minimization scheme employs atomic coordinate optimization for GDP and P_i in advance of b-NVE, where MM simulation with 100-step steepest descent method is followed by that with 400-step conjugate gradient method. The other atomic coordinates are frozen with ibelly algorism. A set of atomic velocities except for P_i were taken over as in the case of other NVE simulations.

Analyses of MD trajectories

Energy, hydrogen bond (HB) formation and root mean square deviation (RMSd) were calculated with the cpptraj module in AmberTools 20 package[28]. Energy was decomposed into three components, namely bonded energy (bond, angle, and dihedral terms), nonbonded one (electrostatic, van der Waals, 1-4 electrostatic and 1-4 van der Waals terms) and kinetic one. Nonbonded energy was calculated under free-boundary condition without distance cutoff.

With regard to each 20-ns NPT MD trajectory, we calculated RMSd to the X-ray crystallography derived Ras-GAP complex structure[24] using the backbone heavy atoms (i.e., C_α, N, C and O). RMSd for generated P_i structures was calculated for non-hydrogen

atoms in P_i structure, which was energetically optimized in vacuum with Hartree-Fock/6-31G* level of theory by using Gaussian 09.[22]

The geometrical criterion of HB formation is as follows: H-X distance was < 3 Å and X-H-Y angle was > 135˚, where X, Y and H denote acceptor, donor and hydrogen atoms, respectively.

Molecular structures were illustrated using Visual Molecular Dynamics (VMD).[30] Error bars are calculated from standard error and indicate 95% confidence interval if there is no annotation.

Results and Discussion

Constructing GDP system from GTP system

We performed 50 independent unbiased 20-ns NPT-MD simulations of Ras-GTP-GAP to obtain statistically dependable results. Considering temporal change of RMSd (**Figure 2**), we assume that Ras-GAP complex reaches structural equilibrium by 20 ns. We then extended each MD trajectory by 106-ps under NVE condition. Each set of atomic coordinates with atomic velocities obtained from the NVE simulation (referred to as f-NVE) was considered to construct a set of atomic coordinates with atomic velocities of the Ras-GDP-GAP system.

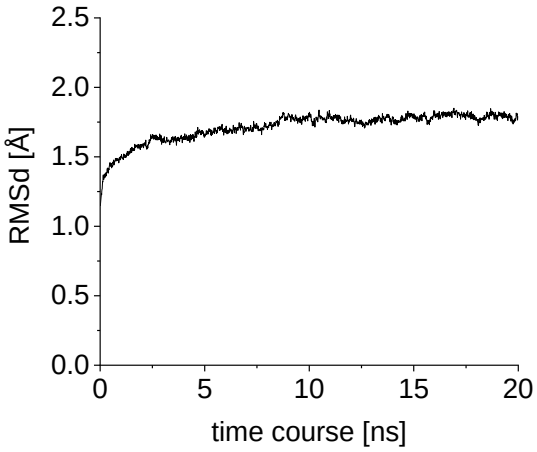

Figure 2. Time course change of root mean square deviation (RMSd) for the Ras-GTP-GAP system. RMSd value at each time point is the average over the 50 independent simulations.

Prior to GTP-GDP conversion by QM/MM simulations, we confirmed for each of the 50 snapshot structures whether the catalytic metal ion (Mg^{2+}) and a reactant water molecule (W_R) are coordinated near the GTP by recalling the results by earlier QM/MM study. In each of the 50 snapshot structures, Mg^{2+} is found around $P_\gamma O_3^-$ and $P_\beta O_2^-$ in GTP (a representative structure is given in **Figure 3A**). Meanwhile, one reactant water molecule was found in the vicinity of P_γ in GTP for the 49 snapshot structures. The remaining one structure loses such a water for the hydrolysis reaction, thus being excluded in the following discussion. We finally obtained 49 snapshot structures to construct atomic coordinates of Ras-GDP-GAP system.

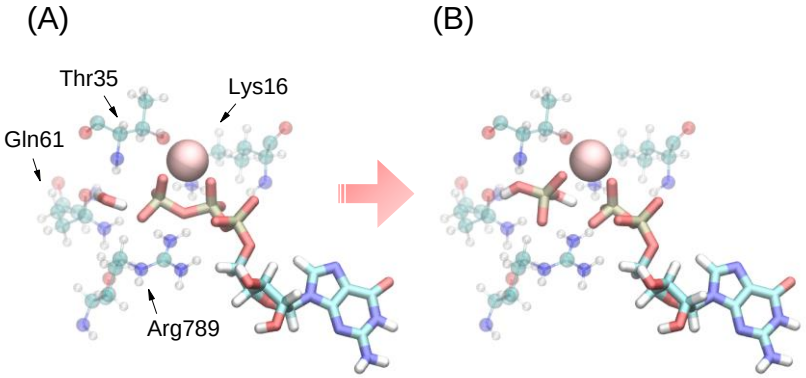

Figure 3. Example of conversion from (A) Ras-GTP-GAP system into (B) Ras-GDP-GAP system by employing the QM/MM simulation. GTP, GDP, inorganic phosphate and reactant water molecule are illustrated by solid sticks. Pink sphere is for Mg^{2+} ion. Catalytic residues (Lys16, Thr35 and Gln61 in Ras; Arg789 in GAP) are shown by transparent ball and stick.

We carried out a QM/MM simulation for each of the 49 snapshot structures and converted GTP and W_R into GDP and P_i (a representative structure is given in **Figure 3B**). RMSd for P_i to the representative P_i structure is 0.21 ± 0.02 [Å], denoting that the molecular configuration is finely generated by our QM/MM simulation. Atomic velocities except for those of P_i were taken over from the 106-ps NVE-MD simulations for Ras-GTP-GAP system (see Materials and Methods for reason for setting atomic velocities of P_i to zero).

Heat generation through relaxation of Coulomb repulsive interaction between GDP and P_i

Each of the 49 sets of atomic coordinates with atomic velocities for Ras-GDP-GAP system was used to following unbiased 106-ps NVE MD simulations (referred to as b-NVE). We first analyzed three energy components, kinetic, bonded and nonbonded energy terms, with regard to GDP with P_i. We can find apparent increase of the kinetic energy of GDP with P_i within the first 0.1 ps (**Figure 4A**). The kinetic energy starts to relax around 0.1 ps and finally reaches to the equilibrium within several picoseconds. Then, increased kinetic energy is accompanied by GDP-P_i generation while it promptly dissipated within several picoseconds. Thus we can suppose this process as a conventional heat generation.

It should be noted that kinetic energy of GDP and P_i increases from 41 to 64 kcal/mol by the first 1 ps (see **Figure 4A**). This value is c.a. several-fold greater than an expected macroscopic estimation for heat generation via triphosphate nucleotide hydrolysis. This observation clearly shows a conceptual gap between macroscopic energy balance of the hydrolysis reaction between equilibrium states and microscopic heat generation at the earlier phase of the hydrolysis reaction.

We confirmed that the above heat generation is brought about by GTP-GDP conversion

by examining the reference system. Each of 106 NVE simulations for the Ras-GTP-GAP system, f-NVE, was simply continued under NVE condition without switching force fields. As shown in **Figure S3**, generation of atomic heats were not observed for this reference system. This result indicates that GTP-GDP conversion brought about the energy relaxation processes illustrated in **Figure 4**.

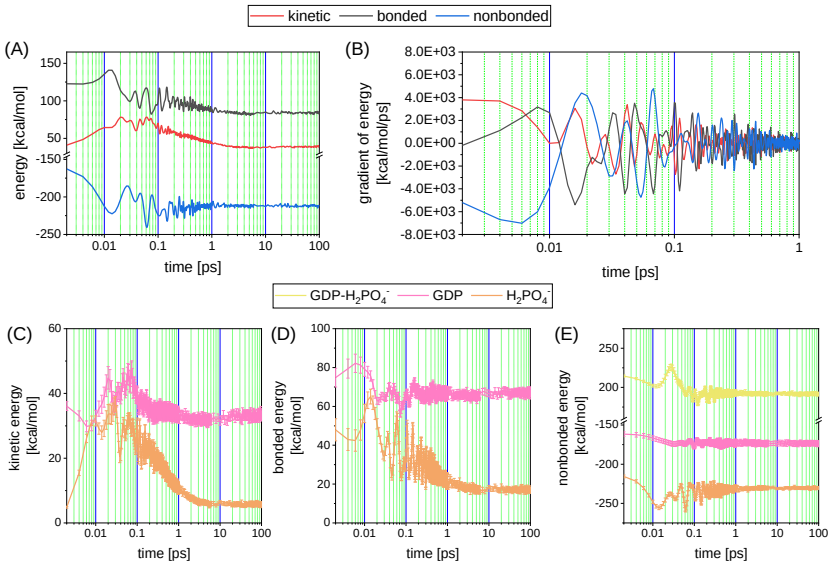

Figure 4. Time course analyses of mechanical energy for Ras-GDP-GAP system. (A) mechanical energy of GDP plus $H_2PO_4^-$ and (B) the time derivative at each time point, where kinetic, bonded and nonbonded energies were shown with red, black and blue lines, respectively. (C)-(E) Energies of GDP and P_i; kinetic, bonded and nonbonded energies were for (C), (D) and (E), respectively. Intra GDP, intra P_i and inter GDP-P_i energies are shown with pink, orange and yellow lines, respectively.

The microscopic heat appears to be generated through the two mechanical steps. The initial heat generation, which occurs within the first 0.01 ps, is accompanied by relaxation of nonbonded energy of GDP with P_i (**Figure 4A** and **B**). The nonbonded energy is mainly attributed to Coulomb energy (see **Figure S4**). Then the above nonbonded energy-kinetic energy conversion directly supports the conjecture that kinetic energy is obtained from reduction of Coulomb repulsive energy.

Simultaneously, decreasing nonbonded energy leads to increasing bonded energy in part. Relaxation of the stored bonded energy starts around 0.02 ps, then bringing about the second heat generation. This step was not referred to in the earlier conjecture and newly found in our atomistic MD simulation, since the conjecture was made from the energy transfer mechanism with a simple physical model rather than complicated full-atomistic one as in this study.

Bonded and nonbonded energies oscillate after 0.1 ps and reach equilibrium within several picoseconds. Recalling timescale of energy relaxation, we can say that the heat generation caused by GTP hydrolysis is classified into fairly high-speed processes in the context of biomacromolecular dynamics.

We further examined mechanical energies for each of GDP and P_i, individually. The

initial heat generation, which occurs by the first 0.01 ps, is attributed to relaxation of nonbonded energy for P_i (**Figure 4C** and **D**). Meanwhile, GDP does not contribute to this heat generation, but rather shows subtle decrease of the kinetic energy and increase of the bonded energy.

During the second heat generation in the period between 0.01 ps to 0.1 ps, bonded energies of P_i and GDP changes into their kinetic energies. At the end of the 106-ps NVE simulation, nonbonded interaction energy acting between GDP and P_i is subtly decreased but kept positive. This energetic stabilization is probably obtained through reorientation of hydrogen in P_i toward $P_\beta O^{2-}$ in GDP. Retained repulsive interaction between GDP and P_i can be explained by a constraint that P_i is prohibited to be released from the Ras by GAP-binding and thus is bound around GDP.

Configurational rearrangement of P-loop via GTP hydrolysis

We next investigate the effect of GTP-GDP conversion on Ras protein by aiming to detect effects of GTP hydrolysis reaction. Since functional regions of Ras are found besides the catalytic sites, energetic terms for Ras functional regions (Switch I, Switch II, α-helix 3 and P-loop; see **Figure 1B**) are discussed to examine the effect of GTP-GDP conversion.

Then, only P-loop shows significant change via the reaction (see **Figures S5**, **S6** and **S7** in Supporting Information for similar analyses for Switch I, Switch II and α-helix 3, respectively). Kinetic and bonded energies of P-loop show immediate increases within 1 ps and gradually return to their initial values (**Figure 5A** and **B**). Meanwhile, nonbonded energy of P-loop start to increase around 0.01 ps and retain the change even after relaxation of other two energy terms (**Figure 5C**).

Increase of nonbonded energy for P-loop, 5.3 kcal/mol at the end of b-NVE, might be obtained from potential energy of GPD plus P_i. This potential energy decreases by 88.3 kcal/mol via the 106-ps NVE MD simulations. Meanwhile decrease of whole potential energy of the Ras-GDP-GAP system is 83.1 kcal/mol (**Figure 6**). The difference between the two values appears to be stored in P-loop in the form of nonbonded energy.

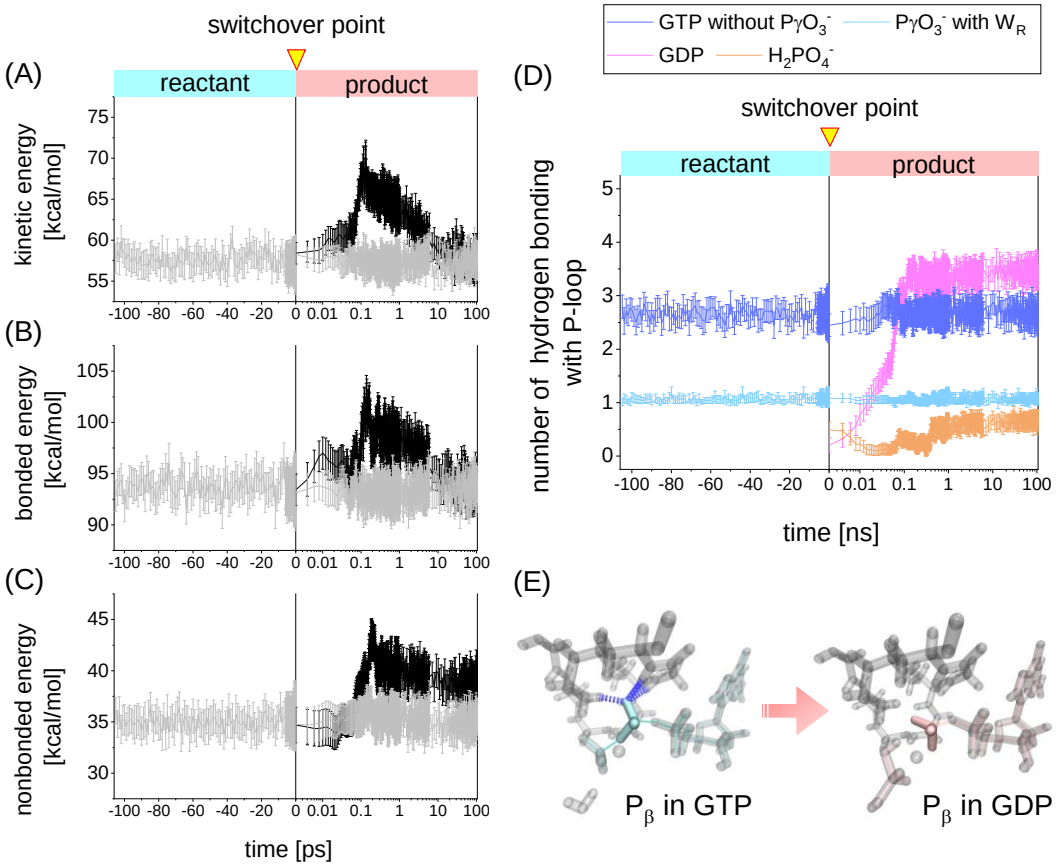

Figure 5. Energetic and structural changes of P-loop in Ras after GTP-GDP conversion. (A)-(C) temporal changes of kinetic, bonded and nonbonded energies, where Ras-GTP-GAP system and Ras-GDP-GAP system are annotated by grey and black lines, respectively. (D) hydrogen bond formation between P-loop and reactant (GTP with reactant water molecule (W_R))/product (GDP and inorganic phosphate (P_i)). Ras-GTP-GAP system is changed into Ras-GDP-GAP system at the switchover point, 0 ps on the time course. (E) Representative illustration for configurational change of P_β via conversion from GTP and GDP.

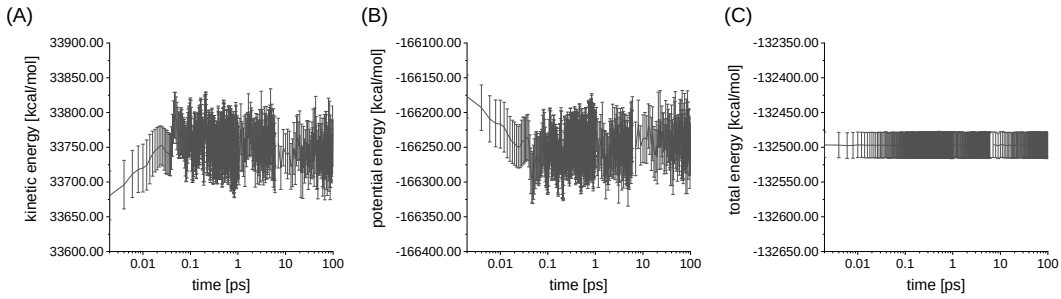

Figure 6. Mechanical energy of Ras-GDP-GAP system. (A) kinetic energy. (B) potential energy (bonded energy plus nonbonded one). (C) total energy (sum of kinetic and potential energies).

The energetic change of P-loop can be explained by rearrangement of intermolecular hydrogen bond formation associated with P-loop, GTP and GDP with P_i. **Figure 5D** represents temporal change of hydrogen bond formation between P-loop and GTP with W_R, and that between P-loop and GDP with P_i. GDP and P_i are separately examined in analyses of hydrogen bond formation with P-loop. As the counterparts in Ras-GTP-GAP system, GTP without $P_\gamma O_3^-$ and $P_\gamma O_3^-$ with W_R were considered in similar hydrogen bond formation analyses.

We can find that GDP finally forms greater number of hydrogen bond with P-loop by c.a. 0.5 than GTP without $P_\gamma O_3^-$. Meanwhile, P_i forms smaller number of hydrogen bond with P-loop than $P_\gamma O_3^-$ with W_R. Thus we suppose that the increasing non-bonded energy of P-loop in Ras-GDP-GAP system results from the rearrangement of P-loop associated

hydrogen bond formation with GDP and P_i.

The number of hydrogen bond between P-loop and GDP shows significant decrease at the force field switchover point. This is due to configurational change of $P_\beta O_3^-$ through modeling the product states (see **Figure 5E** for a representative configurations of $P_\beta O_3^-$). We can find that $P_\beta O_3^-$ is reoriented to break hydrogen bonding with P-loop.

This HB rearrangement occurs within several picoseconds and is still classified into relatively fast process, although the timescale appears to fall in the range of state-of-the-art experimental observation methods for high-speed atomic motions [7,8]. Then the process discussed above could be tested by experimental studies in the future.

It is noted that the energetic and structural changes are sustained even in the following 20-ns unbiased NVE MD simulations (**Figure 7**). The rearrangement of hydrogen bond formation between P-loop and GDP-P_i is expected to furthermore affect those following reaction steps such as Ras-GAP dissociation and/or P_i release from Ras, which would be critical to re-activation process of Ras, GDP-GTP exchange by GEF. However, further investigation for this question is beyond the scope of this study, thus being left for future studies.

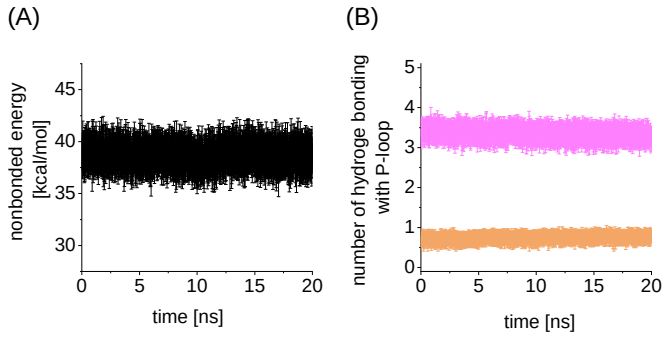

Figure 7. Energetic and structural analyses for extended 20-ns NVE MD simulations for Ras-GDP-GAP system. (A) nonbonded energy of P-loop. (B) hydrogen bond formation between P-loop and products (GDP and P_i, shown by orange and pink lines, respectively).

Effects of GDP-P_i production on P-loop

With employing the SF2MD approach, we observed heat generation by GTP-GDP conversion and the following rearrangement of hydrogen bonds with regard to P-loop and GDP-P_i. Meanwhile, it is elusive so far whether the above structural change is brought about by the generated heat. Then we examine this problem by quenching heat generation with the two different simulation procedures.

Firstly, the kinetic energy was absorbed into thermostat during the initial 1-ps in b-NVE (**Figure 8A** and **B**). Bonded and nonbonded energies of P-loop start to increase around 0.01 ps and only the latter retain the change at the end of the NVE simulations

(**Figure 8C** and **D**). The rearrangement of the hydrogen bond formation was observed even under this simulation condition (**Figure 8E**). It is noted that completion of the rearrangement takes 1 ps, then indicating that this heat absorption delays it by tenfold (compare **Figure 8D** with **Figure 5C**). Thermal quenched motion of GDP with P_i may delay encounter with P-loop and thus retard the rearrangement of hydrogen bond formation. Nonetheless, hydrogen bond rearrangement can still promptly occur under this heat suppression condition by the first 1 ps.

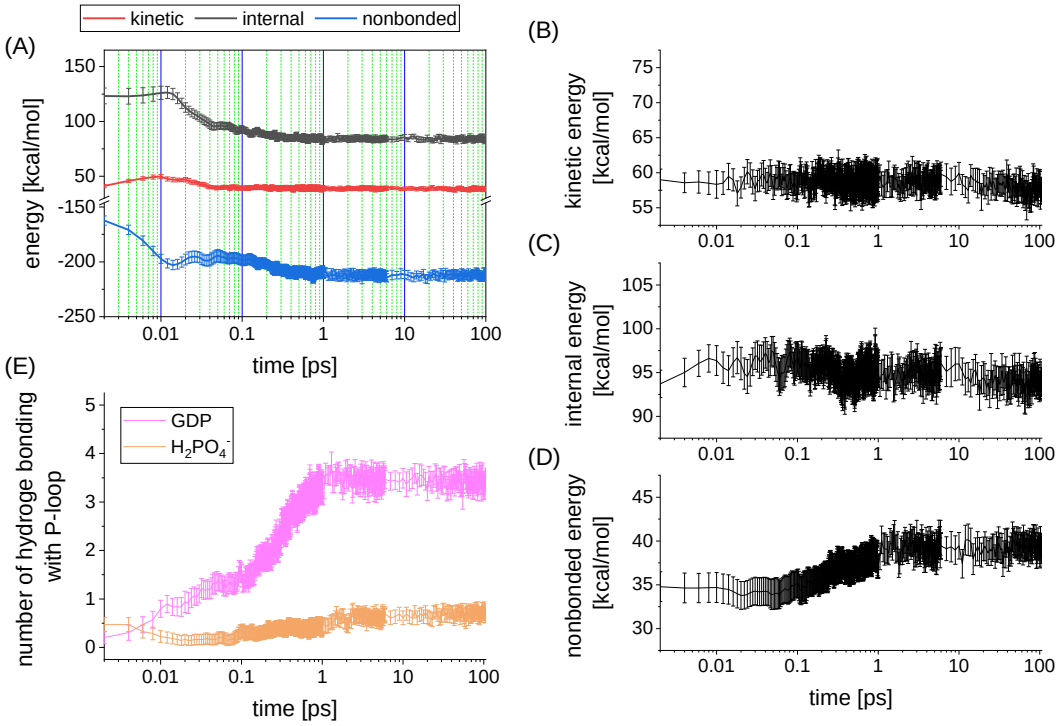

Figure 8. Energetic and structural changes of Ras-GDP-GAP system with heat absorption by employing thermal bath during the first 1 ps. (A) mechanical energy of GDP plus P_i. (B)-(D) kinetic, bonded and nonbonded energies of P-loop. (E) hydrogen bond formation between P-loop and products (GDP and P_i).

Secondly, P_i and GDP are energetically optimized in advance of the b-NVE, aiming to relax the repulsive interaction which can be converted into kinetic energy (**Figure 9**). We find that this simulation suppresses increase of kinetic energies for GDP with P_i and P-loop (**Figure 9A** and **B**). Bonded energy of P-loop appears to be stable in the NVE simulations, while nonbonded energy of P-loop start to increase around 0.1 ps and retain the change at the end of the NVE simulations (**Figure 9C** and **D**). The rearrangement of

the hydrogen bond formation was completed by 1 ps (**Figure 9E**). We find that the number of hydrogen bonds between GDP and P-loop starts from c.a. 3, a relatively large compared to the cases of the unbiased b-NVE and the heat absorption b-NVE discussed just above (compare **Figure 9E** with **Figure 5D**). Such a preformed hydrogen bonding should be due to the preliminary energetic optimization.

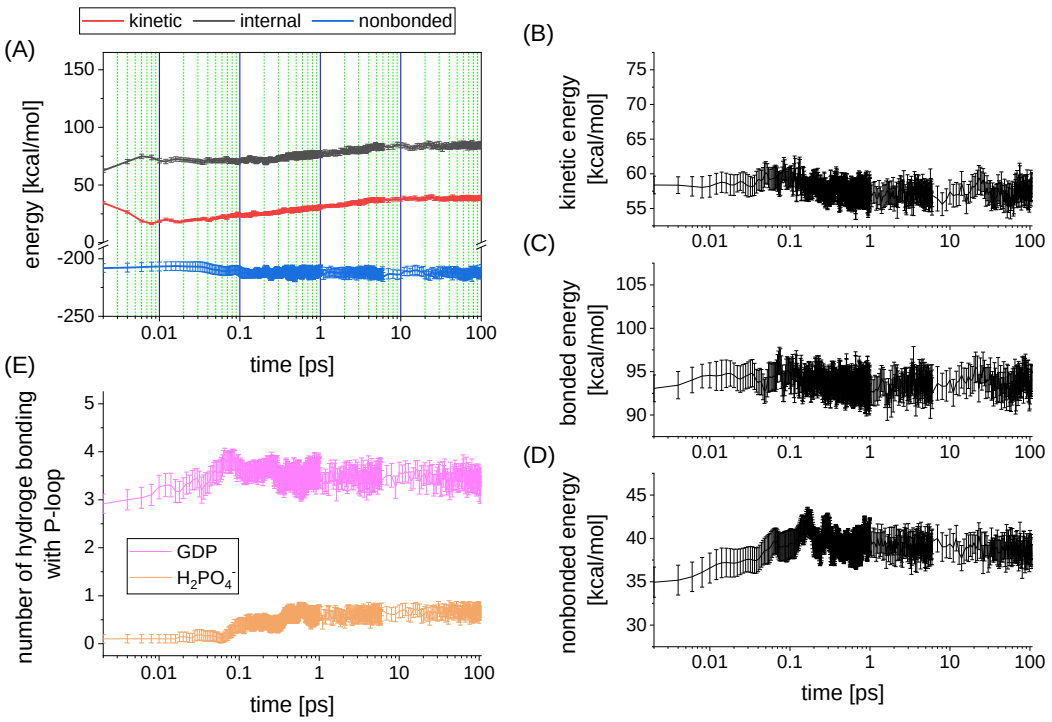

Figure 9. Energetic and structural changes of Ras-GDP-GAP system with preliminary optimization of GDP-P_i configuration. (A) mechanical energy of GDP plus P_i. (B)-(D) kinetic, bonded and nonbonded energies of P-loop. (E) hydrogen bond formation between P-loop and products (GDP and P_i).

Recalling the insights obtained from these two heat-quenching simulations, we can suppose that chemical conversion from GTP to GDP plays central roles in rearrangement of hydrogen bond formation with P-loop, without regard to heat generation via relaxation of repulsive interaction acting between GDP and P_i. This observation for significant effect of chemical conversion could be supported by the earlier experimental study on F_1-ATPase[31], which proposed the functional role of the ATP hydrolysis as inorganic phosphate release. We thus can assume that the functional expression pathways of Ras are fully imprinted in the atomic structure and is directly regulated by interaction with the binding ligand, either GTP or GDP.

Concluding Remarks

In the present study, we examined microscopic process of GTP hydrolysis of Ras-GTP-GAP system by employing MD simulations with SF2MD. Our simulations are designed to verify the earlier conjecture that Coulomb repulsive interactions between GDP and P_i execute work upon Ras protein, and gave physicochemical insights into the heat generation via GTP hydrolysis. Furthermore, we found that the hydrolysis reaction brought about rearrangement of hydrogen bond formation between P-loop in Ras and GDP with P_i. This observation suggests the influence on the following reaction processes

such as P_i release from Ras and Ras-GAP dissociation.

Interestingly, this structural change is essentially promoted by chemical conversion from GTP with reactant water into GDP with Pi, without regard to heat generation via the hydrolysis reaction. As found in the present and in the earlier studies[12,13], kinetic energy generated by chemical reactions rapidly dissipates within several picoseconds and shows substantial fluctuation among individual trajectories. It is suggested that such fast-dissipative energy generated via hydrolysis reaction is unable to certainly activate biologically important molecular dynamics, whose timescales usually fall within microseconds or larger.

The above observation lets us assume that molecular machines working in the cell are designed to work in the cell without remarkably depending on heat generation process itself. The functional expression pathways of ATPase and GTPase may be imprinted into their atomic structures and be finely selected by interaction with the ligands, either ATP or ADP and GTP or GDP under physiological conditions. Such an idea is supported by the earlier experimental study on F_1-ATPase[31], then being interesting clue to understand the functional designs of ATPase and GTPase. This idea also appears to be useful when we design multiscale molecular dynamics simulations, since this kind of chemical reactions could be semi-empirically implemented as chemical conversion between

reactants and products without computationally expensive *ab initio* quantum chemical simulations, as demonstrated in the present study.

We will further examine the above assumption by applying a similar theoretical procedure to other ATPase and GTPase proteins to investigate general roles of such chemical conversions in following mechanical processes in the future.

Supporting Information

The Supporting Information is available. Detailed procedures for MD simulations, Figures and Tables for additional analyses.

Acknowledgements

This work was supported by a Grant-Aid for Scientific Research on Innovative Areas "Chemistry for Multimolecular Crowding Biosystems" (JSPS KAKENHI Grand No. JP17H06353). Parts of MD simulations discussed here were performed by using supercomputers at the Research Center for Computational Science, Okazaki Research Facilities, National Institutes of Natural Sciences, Japan.

Author Information

Corresponding Authors

Ikuo Kurisaki - Graduate School of System Informatics, Kobe University, 1-1 Rokkodai, Nada-ku, Kobe 657-8501, Japan; ORCID: 0000-0003-4519-1093; Email: kurisaki@bear.kobe-u.ac.jp

Shigenori Tanaka - Graduate School of System Informatics, Kobe University, 1-1 Rokkodai, Nada-ku, Kobe 657-8501, Japan; ORCID: 0000-0002-6659-2788; Email: tanaka2@kobe-u.ac.jp

Notes

The authors declare no competing financial interest.

References

1. Howard, J., Molecular Motors: Structural Adaptations to Cellular Functions. *Nature* **1997**, *389*, 561-567.

2. Nogales, E.; Wang, H. W., Structural Mechanisms Underlying Nucleotide-dependent Self-assembly of Tubulin and Its Relatives. *Curr. Opin. Struc. Biol.* **2006**, *16*, 221-229.

3. Gouaux, E.; MacKinnon, R., Principles of Selective Ion Transport in Channels

and Pumps. *Science* **2005**, *310*, 1461-1465.

4. Strunk, B. S.; Karbstein, K., Powering through Ribosome Assembly. *Rna* **2009**, *15*, 2083-2104.

5. Takai, Y.; Sasaki, T.; Matozaki, T., Small GTP-binding Proteins. *Physiol. Rev.* **2001**, *81*, 153-208.

6. Pierce, K. L.; Premont, R. T.; Lefkowitz, R. J., Seven-transmembrane Receptors. *Nat. Rev. Mol. Cell. Bio.* **2002**, *3*, 639-650.

7. Nogly, P.; Weinert, T.; James, D.; Carbajos, S.; Ozerov, D.; Schapiro, I.; Schertler, G.; Neutze, R.; Standfuss, J., Retinal Isomerization in Bacteriorhodopsin Captured by A Femtosecond X-ray Laser. *Acta Crystallogr. A* **2018**, *74*, E170-E170.

8. Shibayama, N.; Sato-Tomita, A.; Ohki, M.; Ichiyanagi, K.; Park, S. Y., Direct Observation of Ligand Migration within Human Hemoglobin at Work. *P. Natl. Acad. Sci. USA* **2020**, *117*, 4741-4748.

9. Salomon-Ferrer, R.; Gotz, A. W.; Poole, D.; Le Grand, S.; Walker, R. C., Routine Microsecond Molecular Dynamics Simulations with AMBER on GPUs. 2. Explicit Solvent Particle Mesh Ewald. *J. Chem. Theory Comput.* **2013**, *9*, 3878-3888.

10. Schweins, T.; Geyer, M.; Scheffzek, K.; Warshel, A.; Kalbitzer, H. R.; Wittinghofer, A., Substrate-Assisted Catalysis as a Mechanism for GTP Hydrolysis of

P21(Ras) and Other Gtp-Binding Proteins. *Nat. Struct. Biol.* **1995**, *2*, 36-44.

11. Ross, J., Energy Transfer from Adenosine Triphosphate. *J. Phys. Chem. B* **2006**, *110*, 6987-6990.

12. Takayanagi, M.; Nagaoka, M., Incipient Structural and Vibrational Relaxation Process of Photolyzed Carbonmonoxy Myoglobin: Statistical Analysis by Perturbation Ensemble Molecular Dynamics Method. *Theor. Chem. Acc.* **2011**, *130*, 1115-1129.

13. Takayanagi, M.; Okumura, H.; Nagaoka, M., Anisotropic Structural Relaxation and Its Correlation with The Excess Energy Diffusion in The Incipient Process of Photodissociated MbCO: High-resolution Analysis via Ensemble Perturbation Method. *J. Phys. Chem. B* **2007**, *111*, 864-869.

14. Maier, J. A.; Martinez, C.; Kasavajhala, K.; Wickstrom, L.; Hauser, K. E.; Simmerling, C., ff14SB: Improving the Accuracy of Protein Side Chain and Backbone Parameters from ff99SB. *J. Chem. Theory Comput.* **2015**, *11*, 3696-3713.

15. Kusalik, P. G.; Svishchev, I. M., The Spatial Structure in Liquid Water. *Science* **1994**, *265* (5176), 1219-1221.

16. Jorgensen, W. L.; Chandrasekhar, J.; Madura, J. D.; Impey, R. W.; Klein, M. L., Comparison of Simple Potential Functions for Simulating Liquid Water. *J. Chem. Phys.* **1983**, *79*, 926-935.

17. Joung, I. S.; Cheatham, T. E., III, Molecular Dynamics Simulations of the Dynamic and Energetic Properties of Alkali and Halide Ions Using Water-Model-Specific Ion Parameters. *J. Phys. Chem. B* **2009**, *113*, 13279-13290.

18. Joung, I. S.; Cheatham, T. E., Determination of Alkali And Halide Monovalent Ion Parameters for Use in Explicitly Solvated Biomolecular Simulations. *J. Phys. Chem. B* **2008**, *112*, 9020-9041.

19. Meagher, K. L.; Redman, L. T.; Carlson, H. A., Development of Polyphosphate Parameters for Use with The AMBER Force Field. *J. Comput. Chem.* **2003**, *24*, 1016-1025.

20. Allner, O.; Nilsson, L.; Villa, A., Magnesium Ion-Water Coordination and Exchange in Biomolecular Simulations. *J. Chem. Theory Comput.* **2012**, *8*, 1493-502.

21. Khrenova, M. G.; Grigorenko, B. L.; Kolomeisky, A. B.; Nemukhin, A. V., Hydrolysis of Guanosine Triphosphate (GTP) by the Ras·GAP Protein Complex: Reaction Mechanism and Kinetic Scheme. *J. Phys. Chem. B* **2015**, *119*, 12838-12845.

22. Frisch, M. J.; Trucks, G. W.; Schlegel, H. B.; Scuseria, G. E.; Robb, M. A.; Cheeseman, J. R.; Scalmani, G.; Barone, V.; Petersson, G. A.; Nakatsuji, H.; Li, X.; Caricato, M.; Marenich, A. V.; Bloino, J.; Janesko, B. G.; Gomperts, R.; Mennucci, B.; Hratchian, H. P.; Ortiz, J. V.; Izmaylov, A. F.; Sonnenberg, J. L.; Williams; Ding, F.;

Lipparini, F.; Egidi, F.; Goings, J.; Peng, B.; Petrone, A.; Henderson, T.; Ranasinghe, D.; Zakrzewski, V. G.; Gao, J.; Rega, N.; Zheng, G.; Liang, W.; Hada, M.; Ehara, M.; Toyota, K.; Fukuda, R.; Hasegawa, J.; Ishida, M.; Nakajima, T.; Honda, Y.; Kitao, O.; Nakai, H.; Vreven, T.; Throssell, K.; Montgomery Jr., J. A.; Peralta, J. E.; Ogliaro, F.; Bearpark, M. J.; Heyd, J. J.; Brothers, E. N.; Kudin, K. N.; Staroverov, V. N.; Keith, T. A.; Kobayashi, R.; Normand, J.; Raghavachari, K.; Rendell, A. P.; Burant, J. C.; Iyengar, S. S.; Tomasi, J.; Cossi, M.; Millam, J. M.; Klene, M.; Adamo, C.; Cammi, R.; Ochterski, J. W.; Martin, R. L.; Morokuma, K.; Farkas, O.; Foresman, J. B.; Fox, D. J. *Gaussian 09 Rev. A.02*, Wallingford, CT, 2016.

23. Wang, J. M.; Wolf, R. M.; Caldwell, J. W.; Kollman, P. A.; Case, D. A., Development And Testing of A General Amber Force Field. *J. Comput. Chem.* **2004**, *25*, 1157-1174.

24. Scheffzek, K.; Ahmadian, M. R.; Kabsch, W.; Wiesmuller, L.; Lautwein, A.; Schmitz, F.; Wittinghofer, A., The Ras-RasGAP Complex: Structural Basis for GTPase Activation And Its Loss in Oncogenic Ras Mutants. *Science* **1997**, *277*, 333-338.

25. Berendsen, H. J. C.; Postma, J. P. M.; Vangunsteren, W. F.; Dinola, A.; Haak, J. R., Molecular-dynamics with Coupling to An External Bath. *J. Chem. Phys.* **1984**, *81*, 3684-3690.

26. Case, D. A.; Cerutti, D. S.; Cheatham, T. E., III ; Darden, T. A.; Duke, R. E.; Giese, T. J.; Gohlke, H.; Goetz, A. W.; Greene, D.; Homeyer, N.; Izadi, S.; Kovalenko, A.; Lee, T. S.; LeGrand, S.; Li, P.; Lin, C.; Liu, J.; Luchko, T.; Luo, R.; Mermelstein, D.; Merz, K. M.; Monard, G.; Nguyen, H.; Omelyan, I.; Onufriev, A.; Pan, F.; Qi, R.; Roe, D. R.; Roitberg, A.; Sagui, C.; Simmerling, C.; Botello-Smith, W. M.; Swails, J.; Walker, R. C.; Wang, J.; Wolf, R. M.; Wu, X.; Xiao, L.; York, D. M.; Kollman, P. A. *Amber 17*, University of California, San Francisco, 2017.

27. Le Grand, S.; Gotz, A. W.; Walker, R. C., SPFP: Speed without Compromise-A Mixed Precision Model for GPU Accelerated Molecular Dynamics Simulations. *Comput. Phys. Commun.* **2013**, *184*, 374-380.

28. Case, D. A.; Belfon, K.; Ben-Shalom, I. Y.; Brozell, S. R.; Cerutti, D. S.; Cheatham, T. E., III ; Cruzeiro, V. W. D.; Darden, T. A.; Duke, R. E.; Giambasu, G.; Gilson, M. K.; Gohlke, H.; Goetz, A. W.; Harris, R.; Izadi, S.; Izmailov, S. A.; Kasavajhala, K.; Kovalenko, A.; Krasny, R.; Kurtzman, T.; Lee, T. S.; LeGrand, S.; Li, P.; Lin, C.; Liu, J.; Luchko, T.; Luo, R.; Man, V.; Merz, K. M.; MIao, Y.; Mikhailovskii, O.; Monard, G.; Nguyen, H.; Onufriev, A.; Pan, F.; Pantano, S.; Qi, R.; Roe, D. R.; Roitberg, A.; Sagui, C.; Schott-Verdugo, S.; Shen, J.; Simmerling, C.; Skrynnikov, N. R.; Smith, J.; Swails, J.; Walker, R. C.; Wang, J.; Willson, L.; Wolf, R. M.; Wu, X.; Xiong, Y.; Xue, Y.; York, D.

M.; Kollman, P. A. *Amber 20*, University of California, San Francisco, 2020.

29. Thiel, W., Semiempirical Quantum-chemical Methods. *Wires Comput Mol Sci* **2014**, *4* (2), 145-157.

30. Humphrey, W.; Dalke, A.; Schulten, K., VMD: Visual Molecular Dynamics. *J. Mol. Graphics Modell.* **1996**, *14*, 33-38.

31. Li, C. B.; Ueno, H.; Watanabe, R.; Noji, H.; Komatsuzaki, T., ATP Hydrolysis Assists Phosphate Release And Promotes Reaction Ordering in F_1-ATPase. Nat. Commun. 2015, 6, 10223.